The Astrophysical Journal, 639:495–509, 2006 March 1

CORONAL HOLES, JETS, AND THE ORIGIN OF ^{3}He-RICH PARTICLE EVENTS

Y.-M. Wang
Code 7672W, E. O. Hulburt Center for Space Research, Naval Research Laboratory, Washington, DC 20375-5352; ywang@yucca.nrl.navy.mil

M. Pick
Observatoire de Paris-Meudon, 92195 Meudon, France; monique.pick@obspm.fr

and

G. M. Mason
Applied Physics Laboratory, Johns Hopkins University, Laurel, MD 20723-6099; glenn.mason@jhuapl.edu
Received 2005 September 6; accepted 2005 November 1

ABSTRACT

Using magnetograph measurements, coronal field extrapolations, and imaging observations, we investigate the solar origins of 25 ^{3}He-rich particle events from the period 1997–2003. In essentially every case we find that the source of the impulsive solar energetic particles (SEPs) lies next to a coronal hole containing Earth-directed open field lines. Averaged over all events, the source-hole separation is only $\sim 4^\circ$ at the photosphere. The source itself is typically a small, flaring active region located between longitudes $\sim$W25 and $\sim$W72. Around the estimated particle injection time, EUV images often show a jetlike ejection aligned with the open field lines. In some cases, a corresponding white-light jet is seen at heliocentric distances $\gtrsim 2\ R_\odot$, similar to those studied earlier by Wang & Sheeley. The jets show a tendency to recur, a behavior that is reflected in the time variation of the measured ^{3}He and Fe particle intensities. We interpret the jets as signatures of magnetic reconnection ("footpoint exchange") between closed and open field lines. On the basis of these findings, we expect ^{3}He enrichments to be observed whenever Earth-connected open field lines undergo footpoint exchanges with nearby active or ephemeral region fields. Because small bipoles emerge continually inside coronal holes, moderate enhancements in the ^{3}He level can occur even when no significant flaring activity is recorded.

Subject headings: Sun: abundances — Sun: corona — Sun: coronal mass ejections (CMEs) — Sun: flares — Sun: magnetic fields — Sun: particle emission

1. INTRODUCTION

Solar energetic particle (SEP) events are conventionally divided into two classes: "gradual" and "impulsive" (for a review of their respective properties, see Reames 1999). Briefly, gradual events are long-lasting, intense, and more closely correlated with coronal mass ejections (CMEs) than with impulsive flares; the bulk of the particle acceleration is thought to occur continuously in the coronal/interplanetary shock waves driven by a large, fast CME. In contrast, impulsive SEP events are smaller and less intense, last less than $\sim$1 day, and appear to originate directly from flaring active regions rather than in CME-driven shocks. Moreover, they are characterized by huge ^{3}He/^{4}He ratios (typically a factor of 10^3 greater than coronal values), by factor of $\sim$10 enhancements in heavy ions such as Ne and Fe, by high ionization states consistent with source region temperatures of $\sim 10^7$ K, and by a dominance of electrons over protons, with the timing of the electron beams being correlated with observations of metric and kilometric type III radio bursts. Whereas the source longitudes of gradual events are distributed almost uniformly over the Sun's disk, impulsive SEPs are focused into a relatively narrow ($\lesssim 30^\circ$) cone and are detectable only when a direct magnetic connection exists to the flare site, which generally requires the latter to be located in the western hemisphere.

Until recently, it was believed that impulsive SEP events do not have associated CMEs. However, Kahler et al. (2001) showed that the injection time of an impulsive SEP event on 2000 May 1 (as deduced from the difference in arrival times between the $\sim$2 and $\sim$20 MeV protons) coincided approximately with the emergence of a fast ($\sim$1000 km s^{-1}), narrow ($\lesssim 20^\circ$) white-light CME above the Sun's northwest limb. They identified a number of other candidate associations and suggested that the CMEs that correspond to impulsive SEP events are relatively narrow and faint. However, a somewhat puzzling aspect of the 2000 May 1 event (not commented on by the authors) was that the associated CME was directed as much as $\sim 40^\circ$ out of the ecliptic plane.

In a related development, Kundu et al. (1994, 1995) and Raulin et al. (1996) found a number of cases in which metric type III bursts observed with the Nançay Radioheliograph coincided spatially and temporally with *Yohkoh* soft X-ray jets. In turn, hot plasma ejections (including both "plasmoids" and jets) with velocities in the range 50–400 km s^{-1} are a characteristic feature of impulsive X-ray flares and are interpreted as resulting from field-line reconnection (Shibata et al. 1995). Since type III bursts are produced by electrons streaming along field lines connected to interplanetary space, these observations suggest that impulsive SEPs may be associated with jetlike ejections that escape from flaring active or ephemeral regions along open field lines (see Kundu et al. 1994; Kahler et al. 2001; Reames 2002).

In a companion paper, Pick et al. (2005) describe five ^{3}He-rich events for which corresponding Nançay Radioheliograph observations are available, allowing a reliable determination of the source location. The events (three of which are also discussed in Klein & Posner 2005) were found to be accompanied by fast, narrow, and relatively faint CMEs, which were detected using the Large Angle and Spectrometric Coronagraph (LASCO) on the *Solar and Heliospheric Observatory* (*SOHO*). Some of these ejections bore a striking resemblance to the white-light jets

TABLE 1
25 Impulsive SEP Events

Date	Hα Flare[a] Location (UT)	EIT Event[b]		LASCO CME[c]		^{3}He/^{4}He[d]	Fe/O[d]	Reference
		Type	Location (UT)	Type	P.A. (UT)			
1997 Nov 24	N21°W63° (12:53)	λ195 flare/ejection	N21°W63° (13:17)	Jet	281° (13:37)	~0.1	~1	1, 6
1998 Aug 18.17	N20°W56° (04:13)	...	...	...	...	6.2	1.19	2
1998 Sep 9.17	S22°W60° (00:10)	...	...	...	...	0.21	1.76	2, 3
1999 Mar 21.17	N25°W26° (04:03)	λ195 flare/jet	N19°W27° (04:36)	?	?	1.67	2.22	3
1999 Jun 18.33	?	λ195 flare/jet	N24°W56° (05:17)	...	...	0.115	1.20	3
1999 Jul 3.70	?	λ195 flare/jet	S14°W56° (16:48)	?	?	0.25	0.72	2
1999 Aug 7.76	N18°W40° (17:28)	λ195 flare/jets	N19°W43° (18:00)	?	?	0.81	1.49	2, 3
1999 Sep 19.61	N20°W70° (14:35)	...	...	...	...	0.02	0.17	2
1999 Sep 30.22	?	λ304 flare/surge	N19°W60° (04:06)	...	...	0.87	1.06	2
1999 Oct 22.75	?	λ195 flare/jets	N09°W72° (16:48)	?	?	0.06	0.44	3
2000 Jan 6.20	?	λ195 flare/ejection	N15°W52° (02:36)	?	?	33.4	1.06	2
2000 Jan 17.13	S18°W46° (04:57)	λ195 flare	S17°W43° (04:52)	?	?	15.9	0.64	2
2000 Jan 18.50	?	λ195 flare/jets	S14°W63° (11:24)	?	?	0.09	0.55	3
2000 Mar 7	S12°W71° (12:31)	λ195 flare	S15°W69° (12:36)	Narrow	262° (12:54)	0.35	2.69	1, 6
2000 May 1.42	?	λ195 flare	N20°W49° (10:24)	Narrow	307° (10:54)	0.06	2.22	1, 2, 3, 4
2000 Jun 4	?	λ195 flare/ejection	S07°W61° (07:13)	Narrow	292° (07:54)	0.31	1.49	1, 6
2000 Aug 22	?	λ195 flare/jet	N22°W40° (00:24)	Wide	301° (00:30)	~1	~1	1, 6
2000 Sep 27.17	N18°W56° (03:10)	λ195 flare/jet	N16°W54° (03:12)	Narrow	323° (03:26)	0.08	0.66	3
2000 Dec 28.00	N12°W38° (02:08)	λ195 flare/jet	N12°W37° (02:12)	?	?	0.16	1.62	3
2002 Aug 19	S11°W27° (10:34)	λ195 flare/ejection	S11°W27° (10:36)	Wide	225° (11:06)	0.05	0.60	6
2002 Oct 5.51	N09°W64° (11:52)	λ195 flare/jet	N09°W65° (12:12)	Jet	271° (12:30)	0.63	1.77	4, 5
2002 Oct 20	S14°W53° (05:29)	λ195 flare/jet	S13°W52° (05:36)	Jet	241° (05:54)	0.17	0.85	6
2002 Dec 12.53	?	λ195 flare/jet	N14°W35° (12:48)	Jet	290° (13:31)	0.48	1.84	4, 5
2003 Mar 2.60	?	λ195 flare/jet	S15°W25° (14:24)	Jet	252° (15:06)	0.65	0.87	5
2003 Mar 17.43	S16°W33° (10:14)	λ195 flare	S17°W35° (10:14)	Jet	254° (11:06)	0.18	0.56	5

[a] From Solar-Geophysical Data (http://www.ngdc.noaa.gov/stp).
[b] The *SOHO* EIT instrument (Delaboudinière et al. 1995) records full-disk images in Fe IX λ171, Fe XII λ195, Fe XV λ284, and He II λ304; however, observations at 12 minute cadence are made routinely only in Fe XII λ195, whose emission peaks at a temperature of $\sim 1.6 \times 10^6$ K.
[c] White-light ejections associated with the flare event were identified in running-difference movies made from LASCO C2 images, whose field of view extends from ~2 to ~6 $R_\odot$ from Sun center. For a description of the *SOHO* LASCO coronagraph, see Brueckner et al. (1995).
[d] The ^{3}He/^{4}He and Fe/O ratios were measured with *ACE* ULEIS at energies of ~0.386 MeV nucleon^{-1} (Mason et al. events) or ~0.5 MeV nucleon^{-1} (all other events). In the case of the 1997 November 24 and 2000 August 22 events, no clear ion injection signature was observed, but ^{3}He/^{4}He and Fe/O were high throughout the day.

References.—(1) Kahler et al. 2001; (2) Mason et al. 2000; (3) Mason et al. 2002; (4) Klein & Posner 2005; (5) Pick et al. 2005; (6) this work.

studied earlier by Wang & Sheeley (2002), whose main characteristics may be summarized as follows: (1) they originate in active regions or bright points located inside or near the boundaries of coronal holes; (2) they often have counterpart jets in the flaring source region, which are visible in images recorded with the *SOHO* Extreme-Ultraviolet Imaging Telescope (EIT); (3) they travel almost ballistically at speeds ranging from ~400 to over 1000 km s^{-1}; (4) they often consist of a succession of sub-ejections; (5) they show a tendency to recur, with the same active-region–coronal-hole system emitting a series of jets over a period of up to several days; and (6) they are most likely triggered by reconnection (footpoint exchange) between the closed active-region loops and the overlying open field lines of the coronal hole.

This paper focuses on the relationship between ^{3}He-rich particle events, open magnetic flux, and coronal jets. Drawing mainly from the lists of Pick et al. (2005), Kahler et al. (2001), and Mason et al. (2000, 2002), we select 25 events whose sources on the solar surface can be located with reasonable certainty (§ 2). We then determine the magnetic field-line topology in the vicinity of each source region by applying a potential-field source-surface (PFSS) extrapolation to magnetograph measurements of the photospheric field (§ 3). After comparing the derived distributions of open flux with He I λ10830 observations of coronal holes (§ 4), we use EIT, LASCO, and Michelson Doppler Imager (MDI) data to further characterize the nature of the source regions and of their coronal ejecta (§ 5). In § 6 we examine the relationship between recurrent jets and the ^{3}He intensities at Earth. Our results are summarized and discussed in § 7.

2. EVENT SELECTION

For this study, we have compiled a list of ^{3}He-rich events that occurred during 1997–2003 and whose source regions we have been able to identify. These impulsive SEP events include the bulk of those described in Mason et al. (2000, 2002) and Pick et al. (2005), as well as those whose CME counterparts are displayed in Figures 3 and 5 of Kahler et al. (2001). The source region of any given event was considered to be reasonably well determined if an Hα flare or a *SOHO* EIT event (flare or ejection) was observed within a few hours of the estimated particle injection time and occurred within the longitude range between ~W20 and ~W90. The injection times were derived from the inverse relationship between the particle velocities and their arrival times, on the assumption of scatter-free propagation (see Mason et al. 2002). In addition, in the case of the Pick et al. (2005) events, injection times deduced for the accompanying energetic (~10–100 keV) electrons were used to identify the associated metric type III bursts in Nançay Radioheliograph images (see also Maia & Pick 2004; Reames et al. 1985).

Table 1 lists the 25 impulsive SEP events selected for this study. The first column gives the date of each event; a decimal date indicates in addition the particle injection time as estimated by Mason et al. (2000, 2002) or Pick et al. (2005). The second

column gives the position and time of the corresponding Hα flare; a question mark means that no event in the appropriate time and longitude window was recorded in the Solar-Geophysical Data prompt reports. The next two columns provide a brief description (nature, location, and time) of the EIT event, with ellipses signifying that no data were available. The fifth column characterizes the corresponding white-light ejection (if observed) as a simple linear "jet," a more complexly structured "narrow CME," or a "wide CME" with an angular extent in excess of $\sim 30^\circ$; the sixth column specifies the average position angle (P.A., measured counterclockwise from the north pole) of the CME and the time when it first appears in the ~ 2–$6\ R_\odot$ LASCO C2 field of view. (Here a question mark means that no ejection could be seen above the west limb within ~ 1 hr of the Hα or EIT event, while ellipses indicate that the coronagraph was not in operation. LASCO C2 images are normally recorded at a rate of 3 per hour.) The seventh and eighth columns give the ^{3}He/^{4}He and Fe/O ratios measured with the Ultra Low Energy Isotope Spectrometer (ULEIS) on the *Advanced Composition Explorer* (*ACE*; see Mason et al. 2000, 2002).

An analysis of related radio observations is presented in Pick et al. (2005). Here we remark only that every event in Table 1 for which the particle injection occurred during the observing time of the Nançay Radioheliograph was accompanied by metric type III emission. These events include those of November 24, September 19, January 18, March 7, May 1, August 19, October 5, December 12, March 2, and March 17.

3. MAGNETIC FIELD-LINE CONFIGURATIONS

We now derive the magnetic topology of the source region associated with each ^{3}He-rich event listed in Table 1. For this purpose, we apply a PFSS extrapolation to photospheric field measurements taken during the 27.3 day Carrington rotation (CR) in which the event occurred. Let r denote heliocentric distance, L heliographic latitude, and ϕ Carrington longitude (measured westward in the direction of the Sun's rotation). In the PFSS model, the coronal field $\boldsymbol{B}(r,\ L,\ \phi)$ is assumed to obey the current-free condition $\nabla \times \boldsymbol{B} = 0$ out to a spherical "source surface" $r = R_{\rm ss}$, where the magnetohydrodynamical effect of the solar wind outflow is simulated by setting the nonradial field components to zero (Schatten et al. 1969). At the inner boundary $r = R_\odot$, B_r is matched to the observed distribution of photospheric flux $B_{\rm phot}(L,\ \phi)$, corrected for line-of-sight projection by assuming that the field is radially oriented at the depth where it is measured (see Wang & Sheeley 1992). All field lines that extend from the photosphere to the source surface are defined to be "open." We henceforth set $R_{\rm ss} = 2.5\ R_\odot$, a value that reproduces the global configuration of He I λ10830 coronal holes throughout the solar cycle (see Wang et al. 1996, Fig. 2).

For the photospheric field, we employ Carrington synoptic maps from the National Solar Observatory (NSO) at Kitt Peak or from the Mount Wilson Observatory (MWO). The MWO magnetograph data were corrected for the saturation of the Fe I λ5250 line profile, as described in Wang & Sheeley (1995) and Ulrich et al. (2002). (The NSO measurements do not require this correction as they were made in the magnetically less sensitive Fe I λ8688 line.) Because they were constructed from observations taken around the time of central meridian passage, the synoptic maps do not capture any magnetic flux that may have emerged subsequently as the source region approached the west limb.

To determine the field-line configuration associated with each event, we trace outward along the magnetic field from an area of the photosphere centered about the source. In addition, we wish to identify the coronal field line that is connected to Earth, wherever its footpoint may lie. This open field line intersects the source surface at the point $(R_{\rm ss}, L_{\rm E}, \phi_{\rm E})$, where $L_{\rm E} = B_0$ is the heliographic latitude of Earth and the longitude $\phi_{\rm E}$ is such that

$$\phi_{\rm E} - \phi_{\rm CM} \simeq \Omega_{\rm Carr}\left(\frac{r_{\rm E} - R_{\rm ss}}{v_w}\right) \simeq 50^\circ\left(\frac{450\ {\rm km\ s^{-1}}}{v_w}\right), \quad (1)$$

where $\phi_{\rm CM}$ is the central meridian longitude, $\Omega_{\rm Carr} \simeq (360^\circ/27.3\ {\rm day})$ is the Carrington rotation rate, $r_{\rm E} = 1$ AU, and v_w is the solar wind speed. The footpoint of the Earth-directed field line is thus located by tracing downward from $(R_{\rm ss}, L_{\rm E}, \phi_{\rm E})$ to the photosphere. In practice, to allow for variations in v_w and for the presence of nonradial motions that act to isotropize the flux distribution beyond $r \sim 2.5\ R_\odot$, we trace a wider bundle of field lines that intersect the source surface over the longitude range W35–W65 and over the latitude band $B_0 - 20^\circ < L < B_0 + 20^\circ$.

It should be emphasized that our magnetic model does not describe the departures from a current-free state that may have led to the eruption, nor does it describe the changes in the field-line configuration that may occur during the eruption. In particular, the open field lines that we derive represent preexisting ones and are not created during the event.

Figures 1–4 display the computed field-line configurations for 24 of the events in Table 1 (the magnetic topology of the 2002 October 5 event is shown in § 5). In each "hairy ball" plot, the source region is marked by a yellow dot, closed loops are coded red, open field lines are green or (if directed into the ecliptic) blue, and the black arrow indicates the position angle of the CME (if present). Black, dark gray, light gray, and white shadings represent areas of the solar surface where $B_{\rm phot} < -10$ G, -10 G $< B_{\rm phot} < 0$, $0 < B_{\rm phot} < +10$ G, and $B_{\rm phot} > +10$ G, respectively. Note that both the green and the blue field lines are directed more or less toward Earth, since we show only the open flux (or a subset thereof) that crosses the source surface in the longitude range W35–W65 and at latitudes less than 20° from the ecliptic plane.

From the figures, we see that each impulsive SEP event originates near an open field region, which in turn is the source of interplanetary field lines that are headed in the general direction of Earth. Averaged over all of our events, the angular separation between the location of the flare/ejection and the open field region is only $\sim 4^\circ$; in some cases, the flaring region is entirely surrounded by open flux. In the events of 1998 September 9 (Fig. 1*c*) and 1999 August 7 (Fig. 2*a*), the separation between the flare and the nearest footpoint area of open flux is as much as $\sim 10^\circ$; however, as they fan outward and bend toward Earth, the open field lines sweep directly over the source region in both cases. The mean source-hole separation of 4° is close to the spatial resolution of the photospheric field maps employed in our PFSS extrapolations; it is also comparable to the error inherent in the neglect of current sheets and other MHD effects (for a comparison between the open field regions derived using different coronal models, see Table I of Sheeley et al. 1989 and Plate 1 of Neugebauer et al. 1998).

As noted above, we have plotted a range of open field lines for each event because the PFSS model does not correctly describe the angular distribution of flux far from the Sun, so that there is some uncertainty in determining which field lines are connected to Earth. In the idealized case in which the photospheric field can be represented by an axisymmetric dipole, a PFSS extrapolation would yield $B_r \propto \sin L$ for the flux distribution at $r \geq R_{\rm ss}$. In fact, however, the heliospheric current sheet located beyond $r \sim 2.5\ R_\odot$ (omitted from the model) will redistribute the flux so

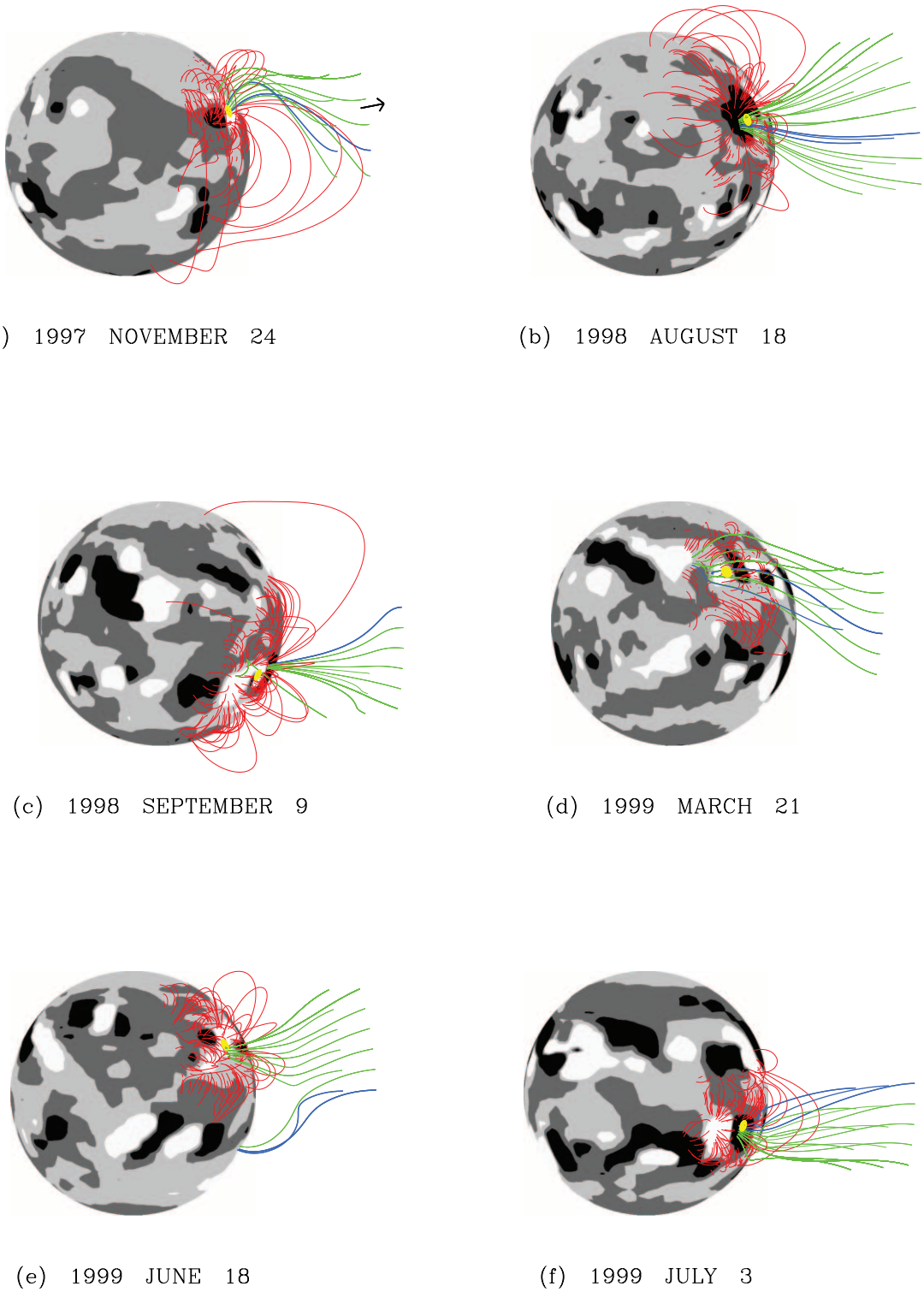

FIG. 1.—Magnetic field-line configurations for six impulsive SEP events from the period 1997–1999. The coronal field associated with each event was derived by applying a PFSS extrapolation to magnetograph measurements, in the form of an NSO or MWO photospheric field map for the relevant CR. The location of the flaring active region (as given in Table 1) is marked by a yellow dot. Open field lines are coded blue if directed into the ecliptic plane and green otherwise; in either case, only those field lines that intersect the source surface at longitudes between W35 and W65 and at latitudes less than 20° from the ecliptic are plotted. Closed field lines are coded red. Black, dark gray, light gray, and white shadings denote areas of the solar surface where $B_r < -10$ G, -10 G $< B_r < 0$, $0 < B_r < +10$ G, and $B_r > +10$ G, respectively. If the event had an associated white-light CME, a black arrow indicates its average, sky-plane projected direction. (*a*) 1997 November 24 (MWO, CR 1929). (*b*) 1998 August 18 (NSO, CR 1939). (*c*) 1998 September 9 (NSO, CR 1940). (*d*) 1999 March 21 (NSO, CR 1947). (*e*) 1999 June 18 (MWO, CR 1950). (*f*) 1999 July 3 (MWO, CR 1951).

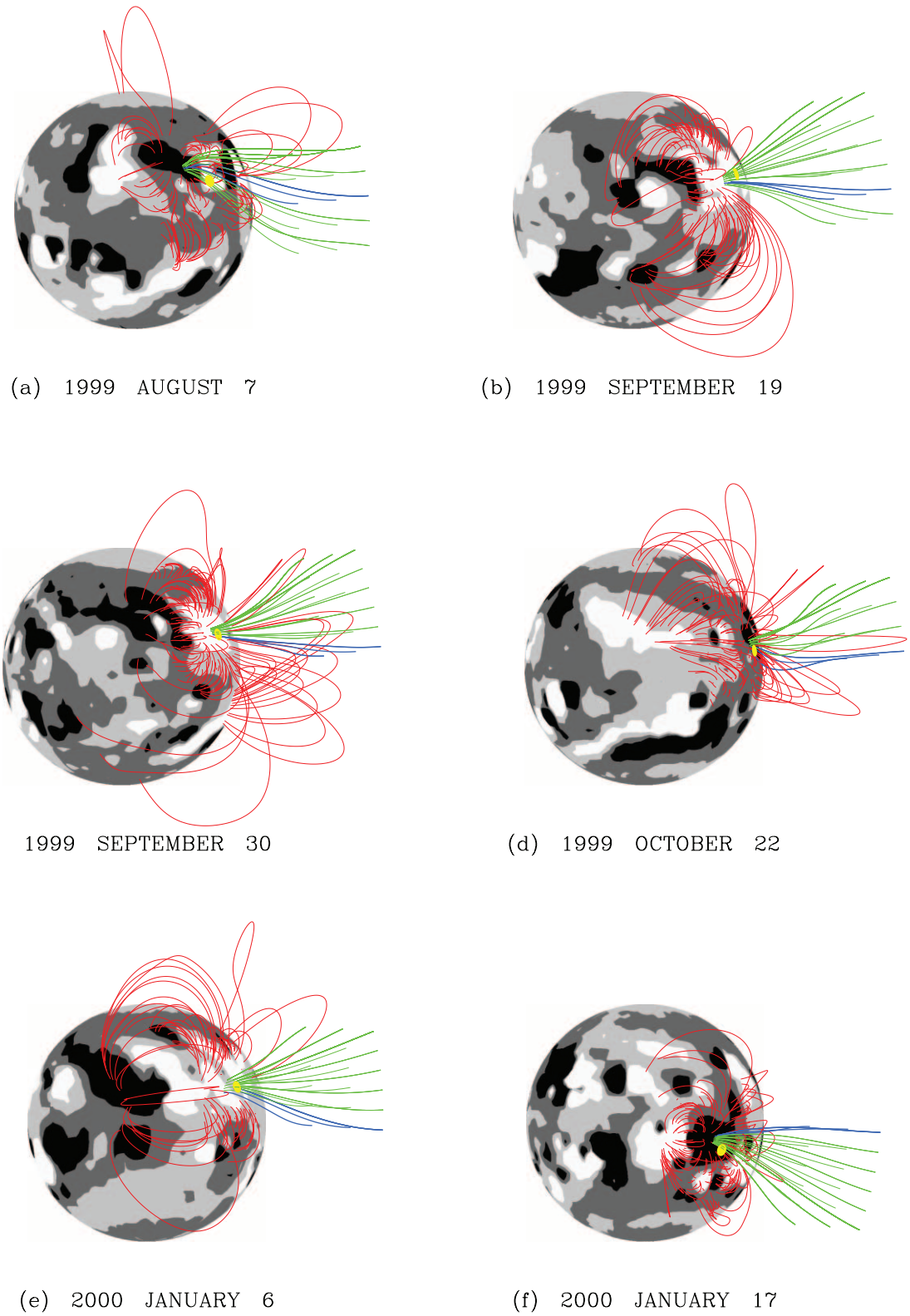

FIG. 2.—Field-line configurations for six impulsive SEP events from the period 1999–2000 (coded as in Fig. 1). (*a*) 1999 August 7 (NSO, CR 1952). (*b*) 1999 September 19 (NSO, CR 1954). (*c*) 1999 September 30 (NSO, 1954). (*d*) 1999 October 22 (NSO, CR 1955). (*e*) 2000 January 6 (NSO, CR 1958). (*f*) 2000 January 17 (NSO, CR 1958).

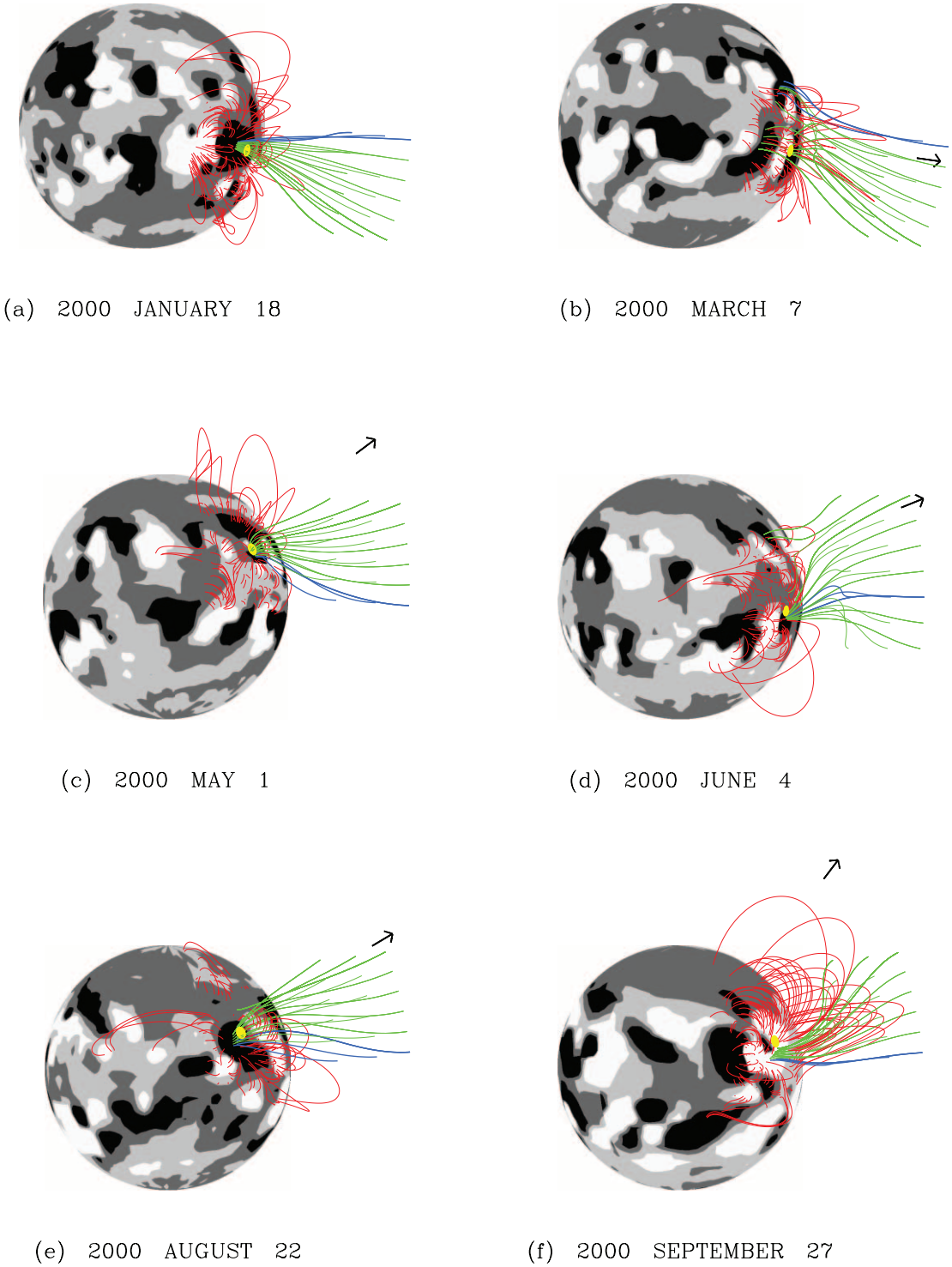

FIG. 3.—Field-line configurations for six impulsive SEP events during 2000 (coded as in Fig. 1). (*a*) 2000 January 18 (NSO, CR 1958). (*b*) 2000 March 7 (NSO, CR 1960). (*c*) 2000 May 1 (NSO, CR 1962). (*d*) 2000 June 4 (NSO, CR 1963). (*e*) 2000 August 22 (NSO, CR 1966). (*f*) 2000 September 27 (MWO, CR 1967).

that it becomes independent of latitude far from the Sun, as observed by *Ulysses* (Balogh et al. 1995; Smith et al. 2001). Thus, from flux conservation, a dipole field line that intersects the source surface at $L = 20^\circ$ would in reality continue to bend equatorward beyond $r \sim 2.5\ R_\odot$, reaching an asymptotic latitude of only $6^\circ.7$.

In most of the impulsive SEP events for which there appears to be an associated white-light ejection, the direction of the CME (indicated by the black arrow) is well away from the ecliptic plane. In the 2000 May 1 event, even the flank of the CME remains above a sky-plane projected latitude of $\sim 25^\circ$. It is evident

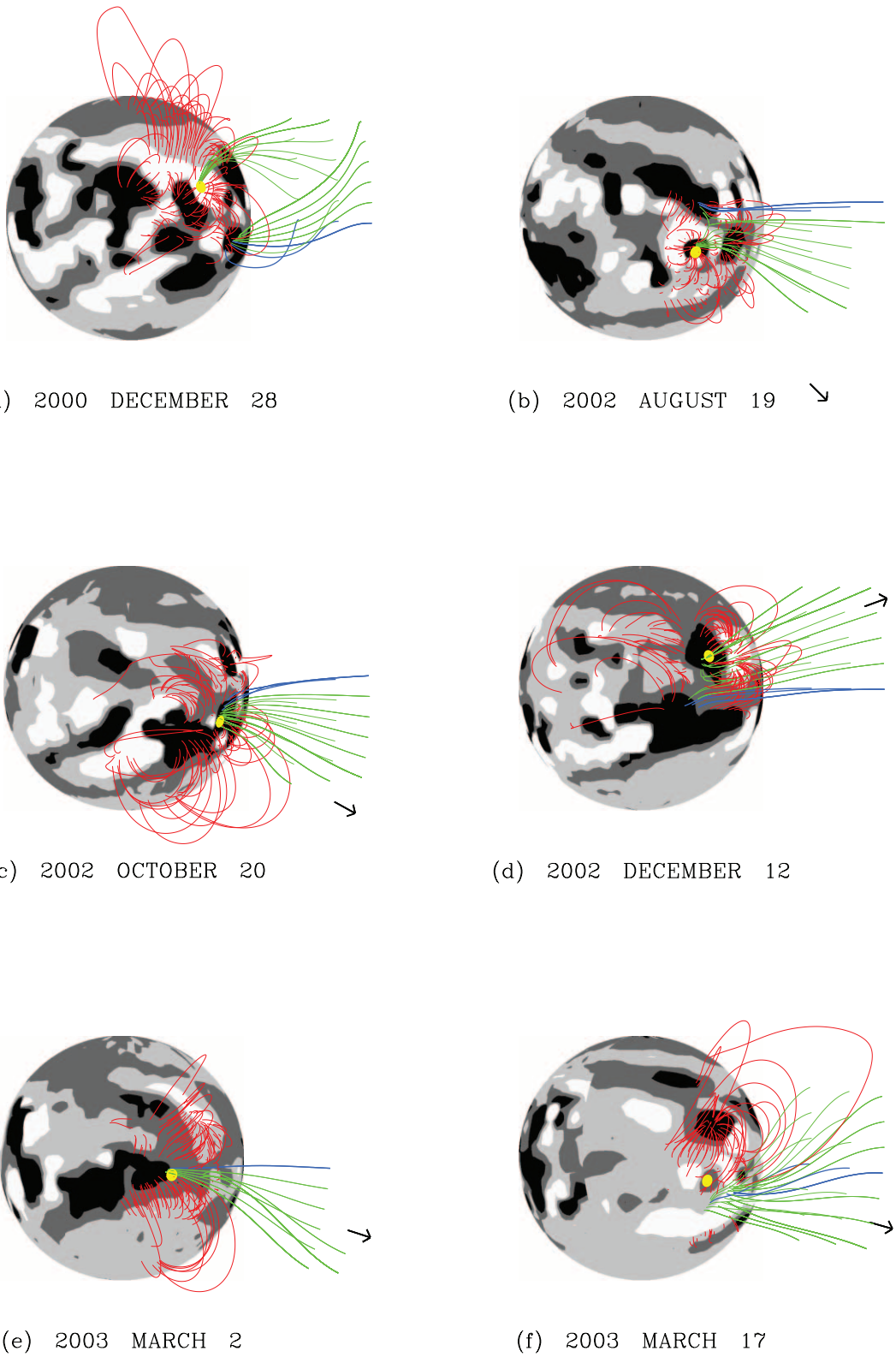

FIG. 4.—Field-line configurations for six impulsive SEP events from the period 2000–2003 (coded as in Fig. 1). (*a*) 2000 December 28 (MWO, CR 1971). (*b*) 2002 August 19 (NSO, CR 1993). (*c*) 2002 October 20 (NSO, CR 1995). (*d*) 2002 December 12 (NSO, CR 1997). (*e*) 2003 March 2 (NSO, CR 2000). (*f*) 2003 March 17 (MWO, CR 2000).

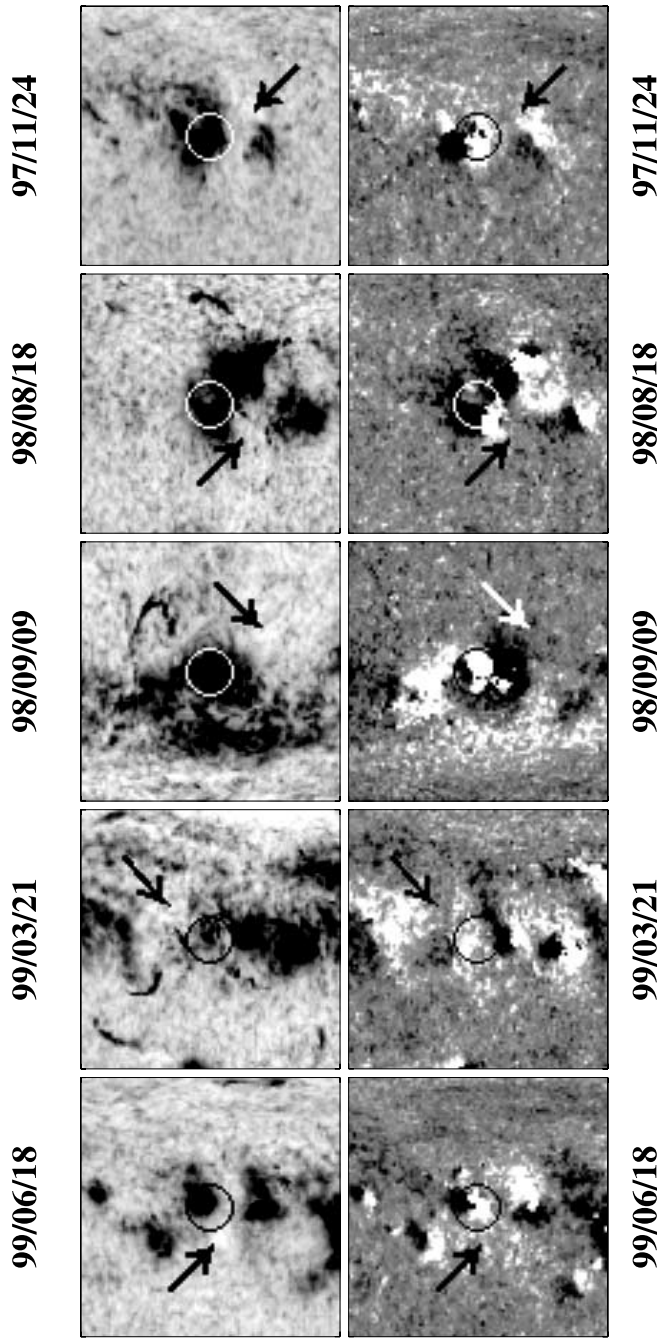

FIG. 5.—Source regions of five impulsive SEP events, as seen in He I λ10830 (*left column*) and in the corresponding Fe I λ8688 magnetograms (*right column*). Each image represents a 90×90 pixel^2 section from a 360×180 NSO Kitt Peak synoptic map. The location of the flaring active region is circled, while an arrow points to the nearby coronal hole. In general, active regions (coronal holes) appear as black (white) areas in He I λ10830; strong negative-polarity (positive-polarity) fields are black (white) in the magnetograms. *First row*: 1997 November 24. *Second row*: 1998 August 18. *Third row*: 1998 September 9. *Fourth row*: 1999 March 21. *Fifth row*: 1999 June 18.

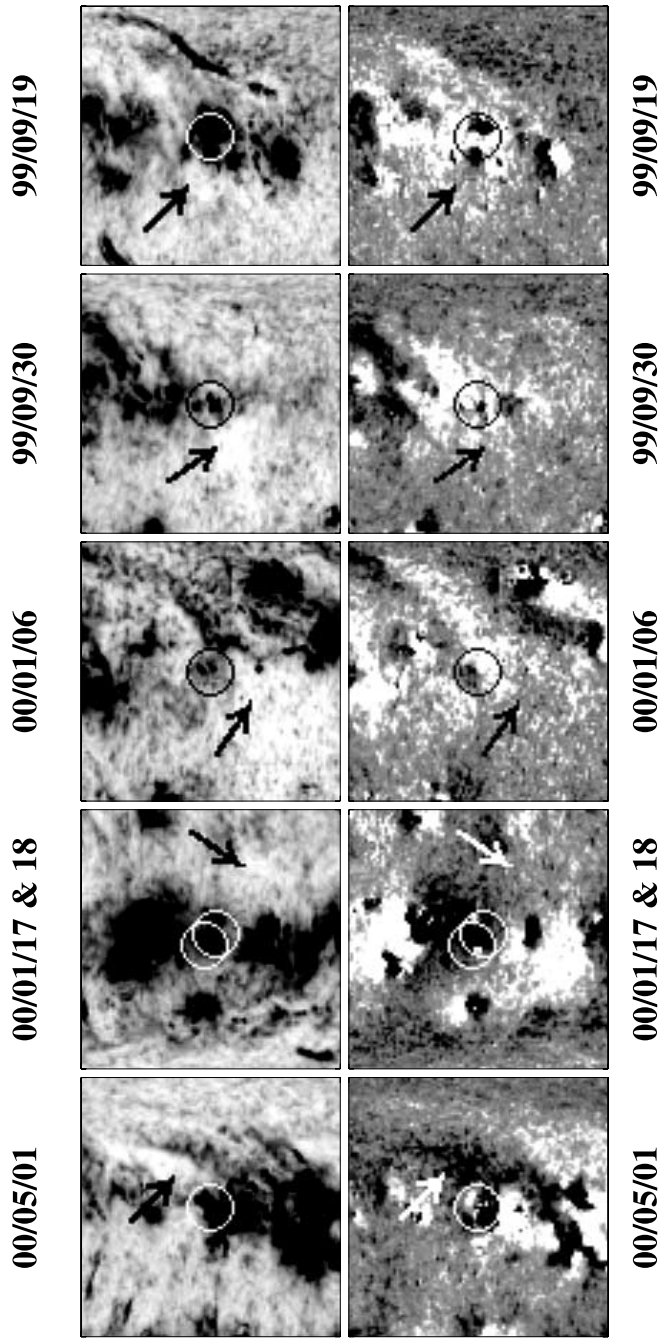

FIG. 6.—Source regions of six impulsive SEP events (for description, see Fig. 5 legend). *First row*: 1999 September 19. *Second row*: 1999 September 30. *Third row*: 2000 January 6. *Fourth row*: 2000 January 17 and 18. *Fifth row*: 2000 May 1.

that the impulsive particles cannot in general originate in the CME itself (see also Pick et al. 2005).

4. RELATION TO CORONAL HOLES

The open field regions derived from the photospheric synoptic maps by the PFSS method are stable structures that existed well before the particle events. Previous studies have demonstrated that such structures generally coincide with coronal holes, which are observed as an absence of emission in soft X-ray and EUV images and as light areas in He I λ10830 spectroheliograms (see, e.g., Levine et al. 1977; Wang et al. 1996; Neugebauer et al. 1998; Luhmann et al. 2002; Schrijver & DeRosa 2003).

An inspection of He I λ10830 data from NSO Kitt Peak shows that, in virtually every case, a coronal hole is present near the source of each particle event, in agreement with the PFSS extrapolations of § 3. In Figures 5–7, we display both the He I λ10830 observations (*left*) and the Fe I λ8688 photospheric field data (*right*) for 16 of our events. Here each image represents a 90×90 pixel^2

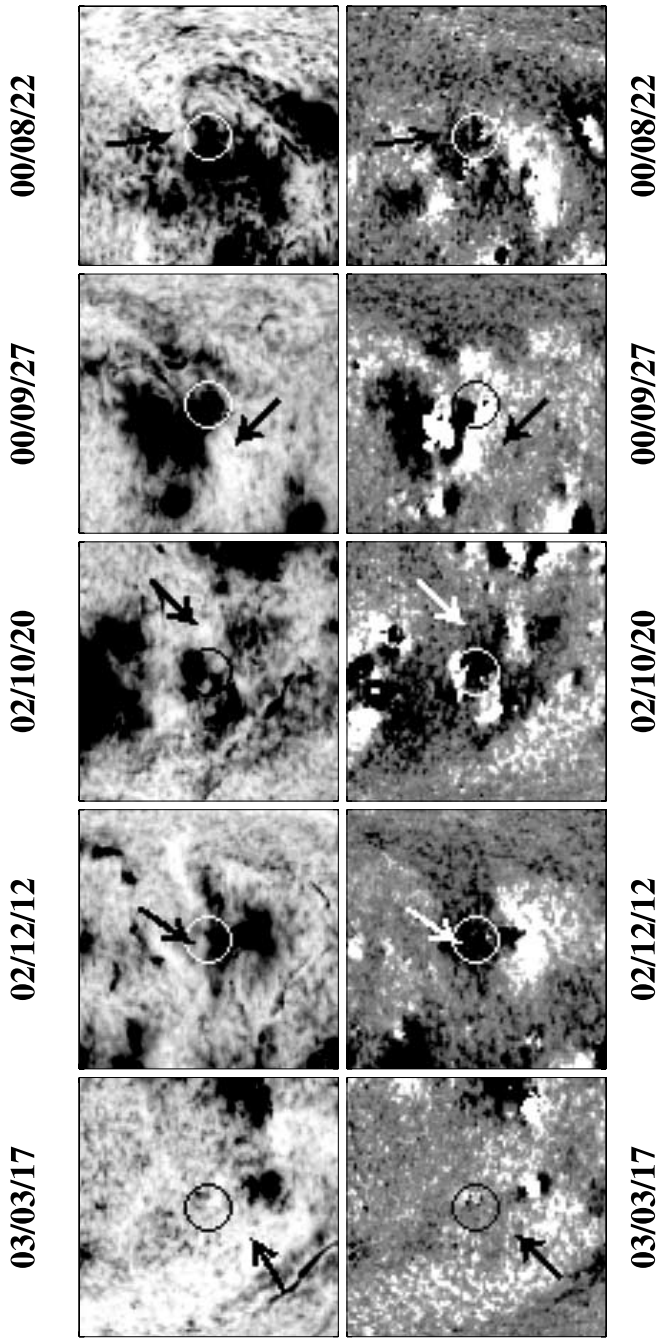

FIG. 7.—Source regions of five impulsive SEP events (for description, see Fig. 5 legend). *First row*: 2000 August 22. *Second row*: 2000 September 27. *Third row*: 2002 October 20. *Fourth row*: 2002 December 12. *Fifth row*: 2003 March 17.

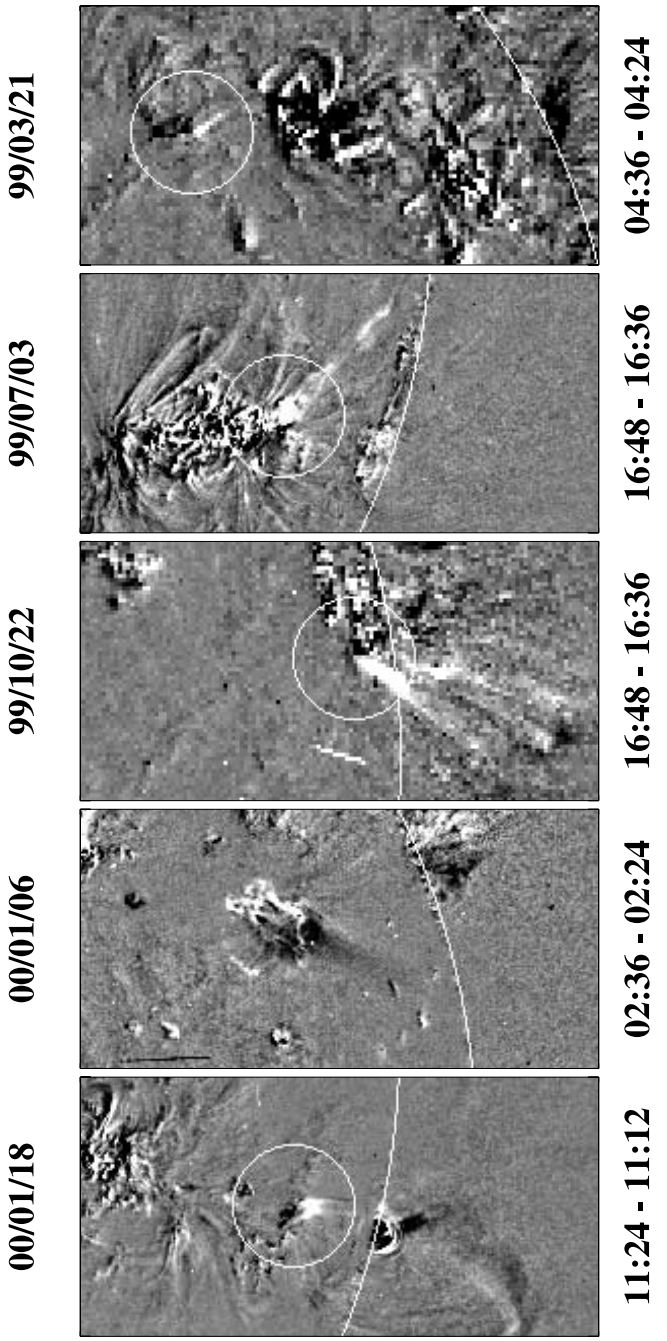

FIG. 8.—EUV jets associated with the impulsive SEP events of (*from top to bottom*) 1999 March 21, 1999 July 3, 1999 October 22, 2000 January 6, and 2000 January 18. Each panel shows the difference between two *SOHO* EIT Fe XII λ195 images taken 12 minutes apart; regions whose emission has increased (decreased) over this time interval appear white (black). Comparison with the corresponding field-line plots (Figs. 1*d*, 1*f*, 2*d*, 2*e*, and 3*a*) suggests that, in every case, the direction of the EIT jet coincides with that of the open field lines rooted near the source region.

section extracted from a 360×180 pixel^2 NSO synoptic map and centered on the source position (as given in Table 1). The source (*circled*) is generally an active region, which appears as a black area in He I λ10830; the location of the nearby coronal hole (*whitish area*) is indicated by an arrow. In some cases, the He I λ10830 coronal hole is "weak," in the sense that it shows only a slight contrast with the surrounding quiet network; however, the PFSS extrapolations confirm that these regions are indeed magnetically open. From the Fe I λ8688 magnetograms, we see that the holes lie within areas dominated by a single polarity, whereas the events themselves originate from regions where strong fields of opposite polarity are in close contact.

That coronal holes are often found alongside active regions is not surprising, given that large magnetic bipoles act as sources of open flux. As the active region fields spread and decay due to supergranular convection, differential rotation, and meridional flow, unipolar regions are created containing embedded open flux/coronal holes. Indeed, the emergence of a large active region is generally accompanied by the appearance of open flux (field lines that extend beyond $r \sim 2.5\ R_\odot$) at its periphery. The formation of coronal holes and polar hole extensions from bipolar

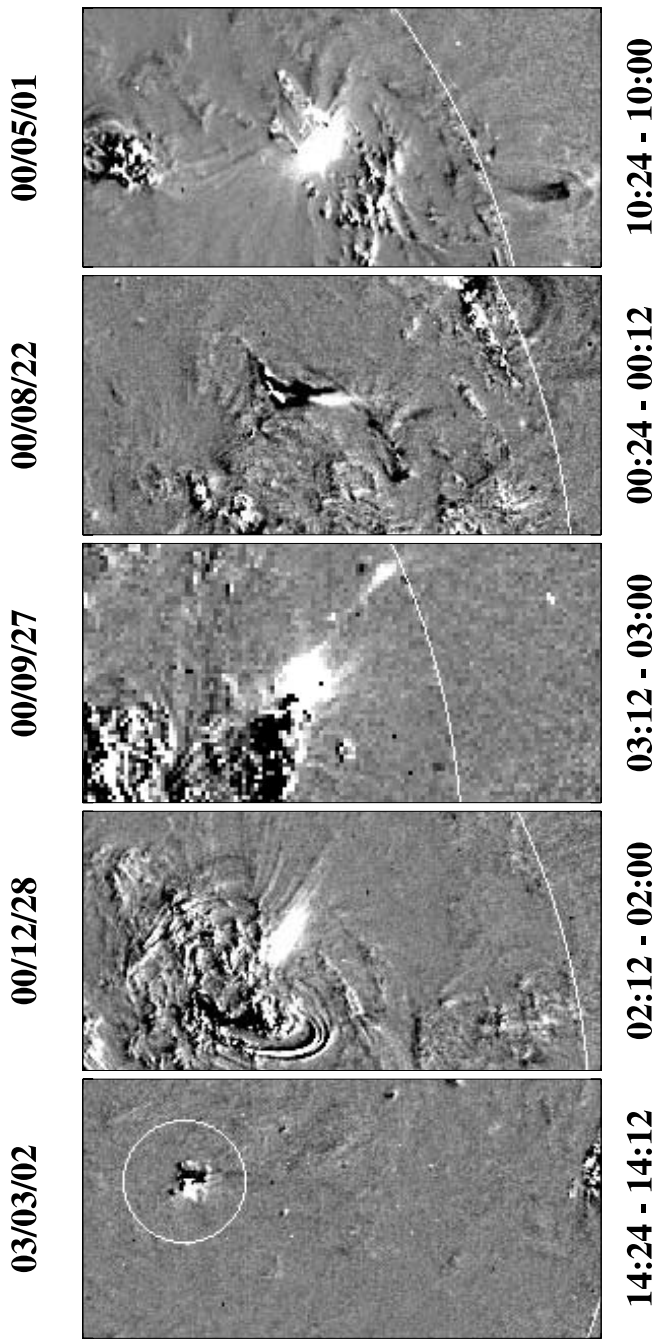

FIG. 9.—EUV flares and/or jets associated with the impulsive SEP events of (*from top to bottom*) 2000 May 1, 2000 August 22, 2000 September 27, 2000 December 28, and 2003 March 2. Again, the ejections appear to be aligned with the open field lines shown in Figs. 3*c*, 3*e*, 3*f*, 4*a*, and 4*e*.

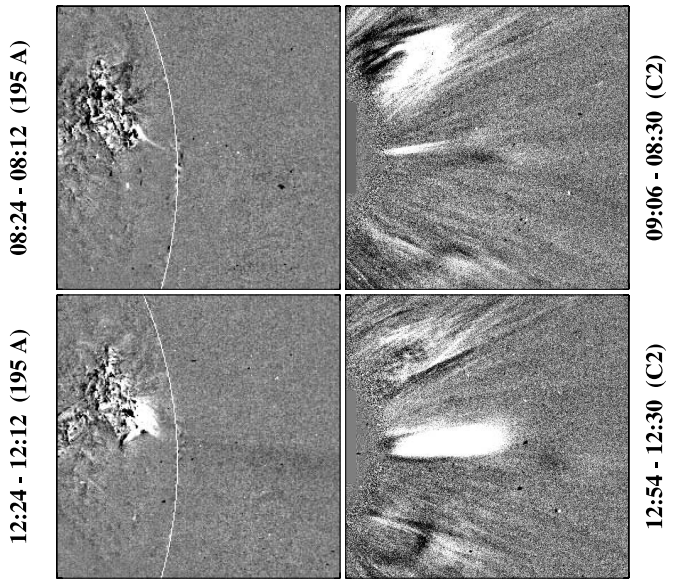

FIG. 10.—Difference images showing two "homologous" LASCO/EIT jet events on 2002 October 5. The Fe XII λ195 jets are at left, while their white-light counterparts beyond $r \sim 2\ R_\odot$ are at right. Note the change in direction of the jets as they propagate from the solar surface to the outer corona (see also Fig. 11). The second eruption is associated with the impulsive SEP event listed in Table 1.

magnetic regions is simulated in Wang & Sheeley (1990b, 2004) and Wang et al. (2000).

5. NATURE OF THE EJECTIONS

As indicated in Table 1, we have identified *SOHO* EIT counterparts for 22 of our impulsive SEP events. Ten of the EUV events are displayed in Figures 8 and 9. In each case, we show the difference between an Fe XII λ195 image taken during the eruption and one taken (typically) 12 minutes earlier. It is apparent that the EUV flare is often accompanied by a collimated ejection or jet. A comparison with the field-line plots in Figures 1–4 shows that the jets are aligned along the open field lines associated with each source region. Thus, in the event of 2000 December 28, where the material appears to be ejected toward high latitudes (fourth panel of Fig. 9), the open field lines in Figure 4*a* are directed poleward near the solar surface but subsequently bend toward the ecliptic. The region identified as the probable source of the 2000 January 18 particle event (bottom panel of Fig. 8) emitted small jets throughout most of the day, all of them pointing westward in the direction of the open field lines (see Fig. 3*a*). In those cases (such as the event of 2000 May 1, shown in the top panel of Fig. 9) in which only an amorphous flare brightening was seen, the jet may have been missed because of the low time cadence of the EIT observations.

As suggested by the fifth column of Table 1, we are unable to associate any single type of white-light CME with our impulsive SEP events. In eight cases, no well-defined ejection was seen to emerge into the $\sim$2–6 $R_\odot$ LASCO C2 field of view above the source region within $\sim$1 hr of the EIT or Hα event. In the remaining cases for which LASCO data were available, the CME was either a linear jet, a more complexly structured narrow

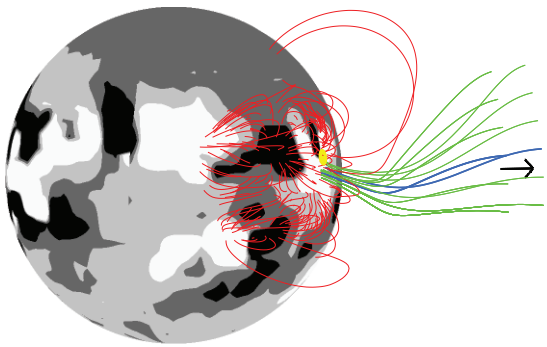

FIG. 11.—Field-line configuration for the source of the 2002 October 5 particle event, derived by extrapolating NSO magnetograph measurements for CR 1994 (for description, see Fig. 1 legend). The open field lines point southward near the solar surface but bend northward at greater heights, thus accounting for the differing orientations of the EIT and LASCO C2 jets in Fig. 10.

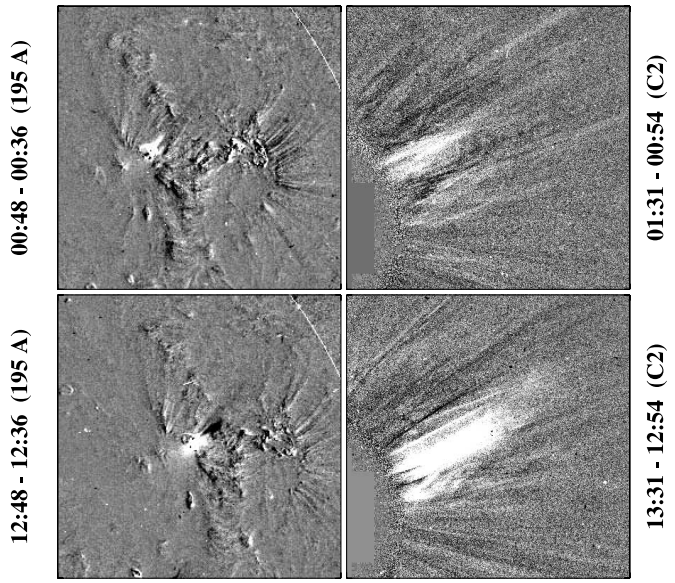

FIG. 12.—Difference images showing two homologous LASCO/EIT events on 2002 December 12. The second eruption is that associated with the impulsive SEP event listed in Table 1. The wishbone shape of the EUV brightening in the top left panel (see also the corresponding panel of Fig. 10) is suggestive of X-point reconnection between closed and open field lines.

CME of angular extent $\lesssim 30^\circ$, or a wide CME. Most of the ejections were narrow and fast ($\sim$500–1000 km s^{-1}), with some showing a tendency to decelerate with heliocentric distance.

The CME associations are especially unambiguous in those cases in which the EUV ejection and its white-light counterpart recur in a homologous way. As an example, Figure 10 (*left column*) shows two EUV jets that were emitted by the same active region near the west limb on 2002 October 5. The second, brighter ejection occurred 4 hr after the first and is associated with the impulsive SEP event listed in Table 1. (In fact, multiple jetlike expulsions were observed during the later flaring episode, which began at $\sim$11:48 UT and lasted until $\sim$12:36 UT; the EIT image at 12:24 UT illustrates the tail end of the jetting activity.) The corresponding LASCO C2 ejections, recorded above the source region about half an hour after each EIT event, are displayed in the right column of Figure 10. Like their respective Fe XII λ195 counterparts, the first white-light jet is faint and narrow (angular extent $\lesssim 3^\circ$), whereas the second is much brighter and wider (angular extent $\sim 9^\circ$) and also has a higher velocity (in excess of 750 km s^{-1}). Especially noteworthy is the difference between the orientations of the EUV jets and their white-light extensions: the former are directed southward, whereas the latter point slightly northward. This change in direction can be understood from the magnetic topology of the source region, displayed in Figure 11. We see that the open field lines rooted next to the flaring region are inclined toward the equator near the solar surface but bend northward at greater heights. A sharp change in the direction of the field is also suggested by the dark depletion trail visible above the bright EUV eruption in the bottom left panel of Figure 10.

Figure 12 shows another pair of homologous eruptions that occurred 12 hr apart on 2002 December 12; again, the second, brighter event is that listed in Table 1. The EUV brightening observed at 00:48 UT has the characteristic "wishbone" shape that is also seen in the first event of 2002 October 5 (top left panel of Fig. 10). This structure (which outlines the separatrix between the different flux systems) is strongly suggestive of reconnection between closed and open field lines at an X-type neutral point

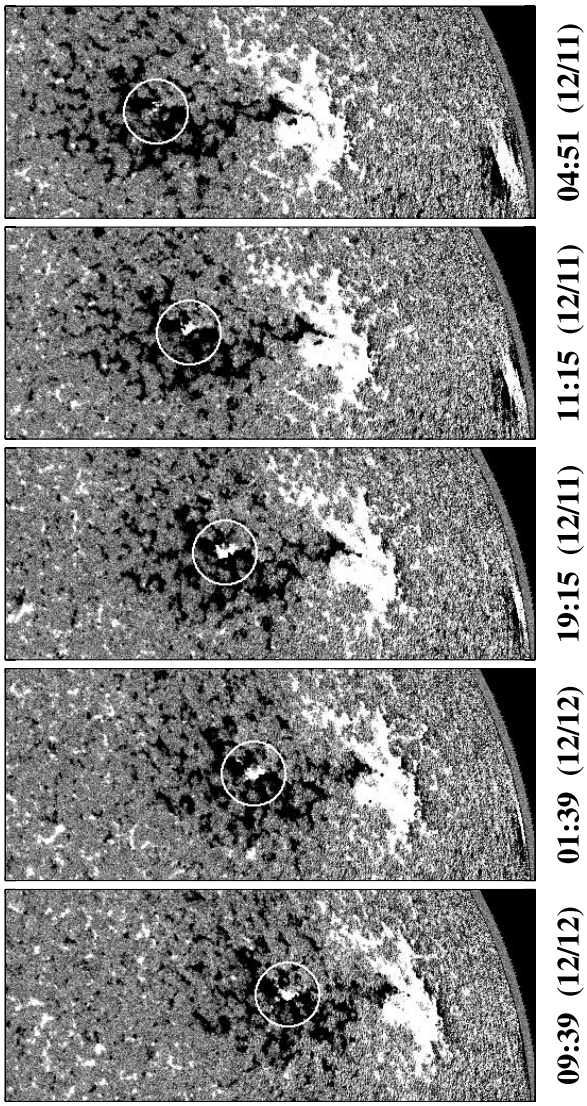

FIG. 13.—Sequence of MDI Ni I λ6768 magnetograms, showing the emergence of positive-polarity flux within a large negative-polarity area during the day preceding the LASCO/EIT ejections of 2002 December 12. The eruptions were centered around the newly emerged bipole. Gray scale for the line-of-sight photospheric field ranges from $B_{\rm los} \leq -20$ G (*black*) to $B_{\rm los} \geq +20$ G (*white*).

(see Fig. 5 in Shibata et al. 1992 or Fig. 6*b* in Wang & Sheeley 2003).

It should be emphasized that most of the counterpart CMEs identified in Table 1 are not directed toward the ecliptic plane (the white-light jet of 2002 October 5, shown in the bottom right panel of Fig. 10, is exceptional in this respect). By implication, the impulsive particles observed at Earth generally do not follow the same trajectory as the bulk of the CME material. We also note that, while linear structures such as those seen in the right panels of Figure 10 can reasonably be interpreted as propagating along preexisting open field lines, those CMEs that we have classified as nonjetlike in Table 1 contain looplike structures and/or filament material and appear to be in the process of creating open flux (some of these CMEs are displayed in Figs. 3 and 5 of Kahler et al. 2001). By definition, the loops that participate in this eruption cannot coincide with the coronal-hole field lines along which the SEPs escape, which are located at the periphery of the CME.

As found in earlier studies (Wang et al. 1998; Wang & Sheeley 2002), Fe XII λ195 jets are commonly observed when magnetic

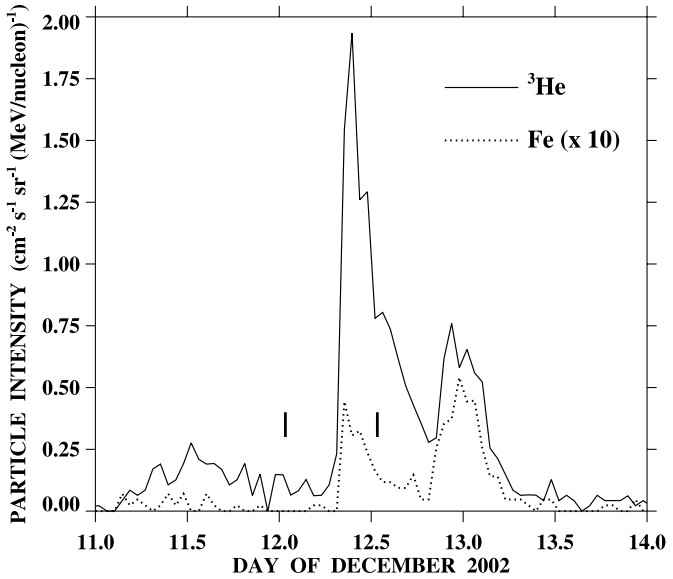

FIG. 14.—Ion intensities in the 0.32–0.45 MeV nucleon^{-1} range measured by *ACE* ULEIS during 2002 December 11–13; units are particles per (cm^2 s sr MeV nucleon^{-1}). *Solid curve:* ^{3}He. *Dotted curve:* Fe. The two peaks correspond to the two LASCO/EIT events displayed in Fig. 12; vertical bars mark the approximate times of the EUV eruptions.

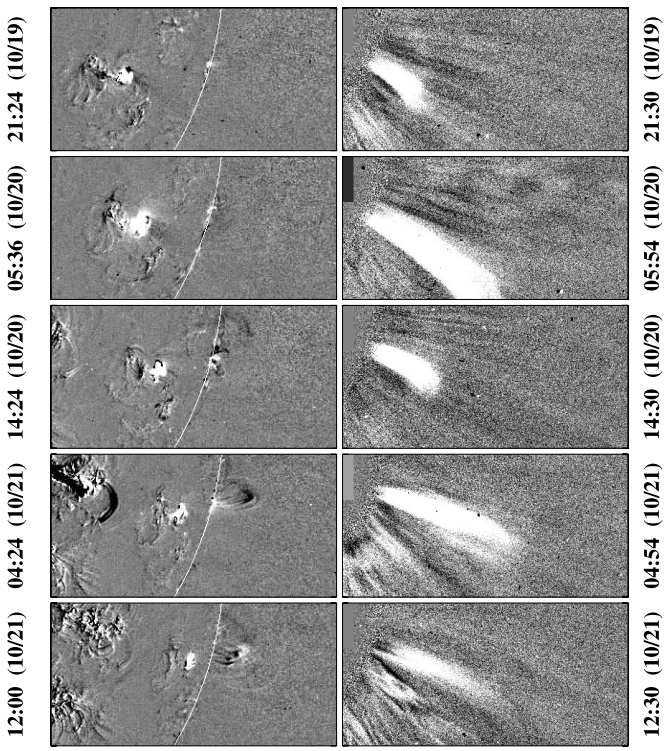

FIG. 15.—Recurrent LASCO/EIT jets from a flaring active-region–coronal-hole system near the southwest limb, 2002 October 19–21. The Fe XII λ195 flares are shown on the left, the corresponding white-light ejections on the right. The first eruption on October 20 is that associated with the event listed in Table 1.

bipoles (in the form of active or ephemeral regions) emerge inside or near coronal holes, which in turn are embedded inside larger unipolar regions. In the case of the EIT jets of 2002 December 12 (Fig. 12), the process that led to these eruptions can be clearly seen in *SOHO* MDI magnetograms. As shown in Figure 13, positive-polarity flux begins to emerge within a large negative-polarity area during the first half of December 11 and continues to do so until the end of the day. When the EUV jets erupt at this location on December 12, the new bipole has fully emerged and may already be undergoing cancellation.

6. RELATION BETWEEN RECURRENT JETS AND PARTICLE ACTIVITY

As already illustrated in the preceding section (see also Wang & Sheeley 2002), active-region–coronal-hole systems show a strong tendency to produce recurrent jets. If these systems are also the sources of impulsive SEPs, then the recurrent behavior should be reflected in in situ particle measurements. Indeed, more than one ion outburst was recorded around the time of the 2002 October 5, October 20, and December 12 events listed in Table 1.

The *ACE* ULEIS spectrogram of inverse ion velocity for 2002 December 12 (based on all ions from H through Fe) shows two slanted tracks, which intersect the horizontal time axis at ~01:00 and ~13:30 UT, respectively. These inferred injection times are roughly consistent with the LASCO/EIT observations of Figure 12. The imprint of both eruptions is also seen in the time variation of the 0.32–0.45 MeV nucleon^{-1} Fe and ^{3}He intensities (Fig. 14): there is a steep rise between ~07:30 and ~09:30 UT as the ions arrive from the first flare, followed by a decline until ~20:00 UT, then a second increase at the end of the day as a result of the later flare. The ~7 hr lag between each LASCO/EIT event and the corresponding rise in the ~0.386 MeV nucleon^{-1} particle intensity would imply a Sun-Earth path length of ~1.46 AU or a wind speed of only ~220 km s^{-1}, assuming scatter-free propagation along the Parker spiral. For comparison, the Solar Wind Electron, Proton, and Alpha Monitor (SWEPAM) on *ACE* measured an average proton bulk speed of ~370 km s^{-1} on December 12. The discrepancy between the inferred and observed values of v_w suggests that the arrival of the ^{3}He and Fe particles may have been delayed somewhat by scattering en route from the Sun. Scattering in the interplanetary medium also acts to broaden the peaks in the particle intensities (see Fig. 14).

During 2002 October 19–21, eight successive LASCO C2 jets were observed above the source region of the October 20 event listed in Table 1. The brighter white-light jets are shown in

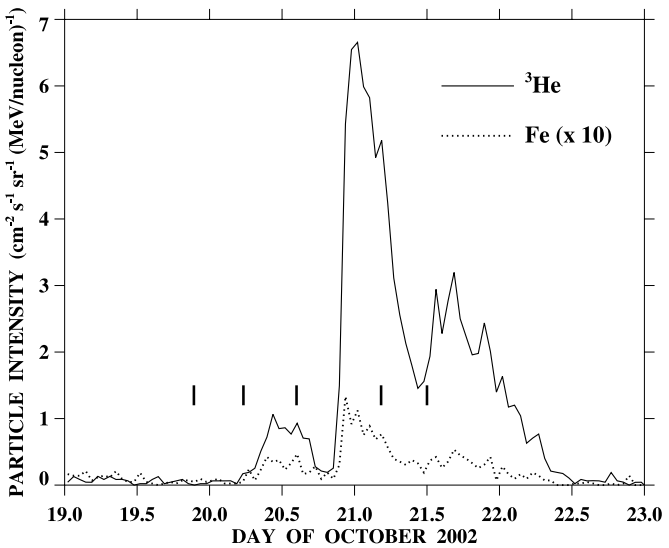

FIG. 16.—Ion intensities in the 0.32–0.45 MeV nucleon^{-1} range measured by *ACE* ULEIS during 2002 October 19–22. *Solid curve:* ^{3}He. *Dotted curve:* Fe. Vertical bars mark the times of the EUV flares displayed in the left column of Fig. 15.

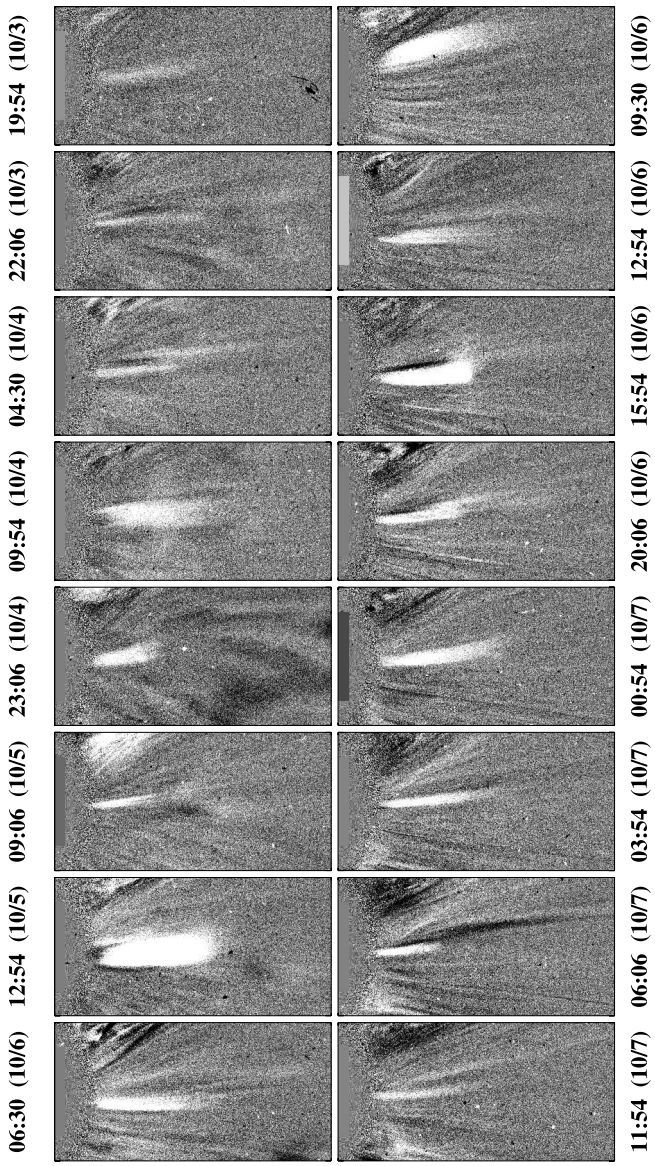

FIG. 17.—The white-light jets shown in Fig. 10 were just two of 16 such events recorded by the LASCO C2 coronagraph from the same flaring active-region–coronal-hole system during 2002 October 3–7. The average sky-plane speed of the jets was close to 700 km s^{-1}.

Figure 15, along with the counterpart Fe XII λ195 events involving a small, flaring active region near the southwest limb. Figure 16 displays the time variation of the ^{3}He and Fe intensities recorded by *ACE* ULEIS at the L1 point. Here we see three distinct peaks, occurring near the middle of October 20, at the end of that day, and around ~16:30 UT on October 21. The first peak follows the LASCO/EIT jet events of ~21:24 UT on October 19 and ~05:36 on October 20, the second and highest peak corresponds to the eruption of ~14:24 UT on October 20, while the final peak is evidently associated with the ejections of ~04:24 and ~12:00 UT on October 21. The ^{3}He and Fe particle intensities remain high through the early part of October 22. That the brightest of the EUV flares (occurring at 05:36 UT on October 20) produced the smallest peak in the ^{3}He flux suggests that field-line connectivity to the source (rather than just the size of the flare) plays a major role in determining the observed enrichment.

The white-light jets of 2002 October 5 (Fig. 10) were just two of many such ejections observed from the same active region

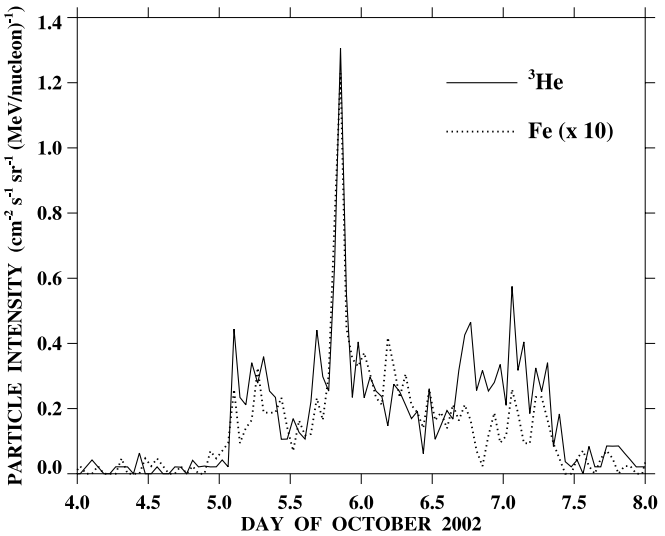

FIG. 18.—Ion intensities in the 0.32–0.45 MeV nucleon^{-1} range measured by *ACE* ULEIS during 2002 October 4–7 (compare Fig. 17). *Solid curve:* ^{3}He. *Dotted curve:* Fe. The highest peak occurs ~8 hr after the flare/jet event displayed in the bottom panels of Fig. 10.

during October 3–7. In Figure 17, we display 16 of these events, some of which involve multiple jets. Figure 18 shows the time variation of the ^{3}He and Fe particle fluxes during this period. The ion intensities rise steeply early on October 5 as magnetic connection to the source is established, remain high over the next two days, and then fall during the first half of October 7. The highest peak, at ~20:30 UT on October 5, corresponds to the event listed in Table 1 and occurs ~8 hr after the flare/jet eruption displayed in the bottom panels of Figure 10.

Only a relatively small fraction of the impulsive SEP events in Table 1 were accompanied by white-light jets, perhaps because such ejections are generally very faint and can only be detected when close to the sky plane. In contrast, EUV jets were identified in the majority of our events, despite the low time cadence of the EIT observations. Running-difference movies made from Fe XII λ195 images suggest that small flares and jets are commonplace. As an example, the source region of the 2000 January 18 particle event and its immediate vicinity continually produced minijets over an extended period beginning on the previous day; the ^{3}He level remained enhanced throughout this time. More generally, the fact that flaring EUV bright points are found throughout coronal holes may explain why enhanced levels of ^{3}He and Fe often occur outside major particle events.

7. SUMMARY AND DISCUSSION

This study has focused on the solar origins of impulsive, ^{3}He-rich SEPs. From our analysis of 25 such events, a number of clear patterns have emerged concerning the nature of the source regions, which show remarkably consistent properties. Our main results may be summarized as follows:

1. From a PFSS extrapolation of the observed photospheric magnetic field, we find that Earth-directed open field lines are rooted next to the source of each impulsive event. The average angular separation between the source location and the open field region is ~4°. The open flux is *preexisting* and not created during the event.

2. The open field region alongside each source generally coincides with a He I λ10830 coronal hole.

3. The source itself is typically a small, flaring active region. In the 11 cases for which no Hα flare was recorded, EUV images

from *SOHO* EIT nevertheless showed a sudden, localized brightening near the predicted particle injection time. All of our sources were located in the longitude range ~W25–W72 and at latitudes $|L| \lesssim 24^\circ$.

4. In 13 of the 21 cases for which Fe XII λ195 observations were available, the EUV flare was accompanied by a narrow ejection aligned in the direction of the open field lines. We surmise that such jets would have been found for even more of our particle events had the EIT images been taken at higher cadence.

5. The white-light ejections associated with our events (if present) ranged from linear structures representing the outer coronal extensions of the EIT jets to CMEs with widths much greater than 30°. The majority of the LASCO counterparts were narrow and fast (~500–1000 km s^{-1}).

6. The EUV jets and their white-light counterparts showed a tendency to recur, with the same active-region–coronal-hole system emitting a series of jets over a period of a day or more. The ^{3}He and Fe particle intensities showed corresponding long-lived enhancements.

Our conclusion that impulsive SEPs originate at the interface between active regions and coronal holes is consistent with the results of Zwickl et al. (1978), who found that ^{3}He-rich events during the declining phase of solar cycle 20 tended to occur in the slow solar wind preceding the onset of a high-speed stream. Slow wind, which is correlated with rapid field-line divergence at the Sun, originates not only from coronal hole boundaries but also from the interiors of small coronal holes (Wang & Sheeley 1990a). Thus, while ^{3}He-rich events are indeed expected to be embedded in the low-speed wind associated with hole boundaries, they need not be followed by high-speed streams during solar maximum, when the large polar holes are replaced by a diverse collection of smaller holes concentrated in the sunspot latitudes.

The jets can be interpreted as a signature of magnetic reconnection between the active region fields and the open flux from the nearby coronal hole (see Shibata et al. 1992; Raulin et al. 1996; Wang & Sheeley 2002). In this footpoint exchange process, plasma is transferred from closed to open field lines and escapes into the heliosphere in the form of a narrow, collimated ejection. As argued by Reames (2002), although reconnection among closed loops might likewise lead to acceleration and fractionation, the resulting energetic particles would remain trapped and precipitate toward the photosphere.

The observed ^{3}He/^{4}He and Fe/O ratios show large variations from event to event, even when the outbursts originate from the same active region (see Figs. 14, 16, and 18). This variability (which shows no simple relationship to the size or brightness of the EUV flare) suggests that the fractionation process has a strong spatial dependence, as is perhaps consistent with the highly localized nature of field-line reconnection.

The absence of any observable white-light ejection in at least eight of our events is consistent with previous findings that impulsive SEPs need not be accompanied by the expulsion of significant amounts of mass. (In order to be detected with the LASCO coronagraph, an ejection near the sky plane must have a total mass $\gtrsim 10^{11}$ g; large CMEs have masses $\gtrsim 10^{15}$ g.) Even in those cases in which a CME was identified, the ejection was usually directed away from the ecliptic, so that the particles arriving at Earth clearly did not follow the same trajectory as the bulk of the CME material. This tendency for the ^{3}He-rich events to occur at the periphery of the CME is hardly surprising, given that footpoint exchanges between the active region and the coronal hole take place only at the boundary of the closed field region.

That impulsive SEP events generally involve the expulsion of at least a small amount of mass is indicated by the existence of white-light extensions to some of the EUV jets (see also Wang et al. 1998; Wang & Sheeley 2002). The outer coronal jets tend to be very faint and are detectable only when located close to the sky plane.

In general, we expect impulsive SEPs to be observed whenever an open field line connected to the spacecraft undergoes a footpoint exchange with a nearby bipole. Given that small bipoles (in the form of ephemeral regions/EUV bright points) emerge continually inside coronal holes, such footpoint exchanges should occur frequently. We can thus understand why the ^{3}He and Fe intensities often show moderately enhanced levels even when no significant flaring activity is observed.

In closing, we note that the field-line tracing method used here provides a simple and effective tool for locating—and even predicting—the sources of impulsive SEP events at Earth. The procedure works because the particles follow preexisting open field lines, which are well represented by the PFSS model. In contrast, it is inadequate to assume that the source longitude coincides with ϕ_E (the base of the Parker spiral as given by eq. [1]), because the inner coronal field is highly nonradial and controls the particle motion below $r \sim 2.5\ R_\odot$. Ideally, field-line tracing should be combined with high-cadence EUV and decimetric/metric radio imaging to pinpoint the source location; Hα flare records alone are insufficient for this purpose and may even be misleading.

We are indebted to the EIT, LASCO, MDI, and ULEIS teams for the use of their spacecraft observations. The NSO Kitt Peak data were produced cooperatively by NSF/NOAO, NASA/GSFC, and NOAA/SEC; the MWO photospheric field maps were provided by R. K. Ulrich. Y.-M. W. thanks M. Pick and R. Grappin for hosting a 3 month visit to the Observatoire de Paris-Meudon. This research was supported by NASA and ONR/NRL.

REFERENCES

Balogh, A., Smith, E. J., Tsurutani, B. T., Southwood, D. J., Forsyth, R. J., & Horbury, T. S. 1995, Science, 268, 1007
Brueckner, G. E., et al. 1995, Sol. Phys., 162, 357
Delaboudinière, J.-P., et al. 1995, Sol. Phys., 162, 291
Kahler, S. W., Reames, D. V., & Sheeley, N. R., Jr. 2001, ApJ, 562, 558
Klein, K.-L., & Posner, A. 2005, A&A, 438, 1029
Kundu, M. R., Raulin, J. P., Nitta, N., Hudson, H. S., Shimojo, M., Shibata, K., & Raoult, A. 1995, ApJ, 447, L135
Kundu, M. R., Strong, K. T., Pick, M., White, S. M., Hudson, H. S., Harvey, K. L., & Kane, S. R. 1994, ApJ, 427, L59
Levine, R. H., Altschuler, M. D., Harvey, J. W., & Jackson, B. V. 1977, ApJ, 215, 636
Luhmann, J. G., Li, Y., Arge, C. N., Gazis, P. R., & Ulrich, R. 2002, J. Geophys. Res., 107, 3
Maia, D. J. F., & Pick, M. 2004, ApJ, 609, 1082
Mason, G. M., Dwyer, J. R., & Mazur, J. E. 2000, ApJ, 545, L157
Mason, G. M., et al. 2002, ApJ, 574, 1039
Neugebauer, M., et al. 1998, J. Geophys. Res., 103, 14587
Pick, M., Mason, G. M., Wang, Y.-M., Tan, C., & Wang, L. 2005, ApJ, submitted
Raulin, J. P., Kundu, M. R., Hudson, H. S., Nitta, N., & Raoult, A. 1996, A&A, 306, 299
Reames, D. V. 1999, Space Sci. Rev., 90, 413
———. 2002, ApJ, 571, L63
Reames, D. V., von Rosenvinge, T. T., & Lin, R. P. 1985, ApJ, 292, 716
Schatten, K. H., Wilcox, J. M., & Ness, N. F. 1969, Sol. Phys., 6, 442
Schrijver, C. J., & DeRosa, M. L. 2003, Sol. Phys., 212, 165
Sheeley, N. R., Jr., Wang, Y.-M., & Harvey, J. W. 1989, Sol. Phys., 119, 323
Shibata, K., et al. 1992, PASJ, 44, L173
———. 1995, ApJ, 451, L83

Smith, E. J., Balogh, A., Forsyth, R. J., & McComas, D. J. 2001, Geophys. Res. Lett., 28, 4159
Ulrich, R. K., Evans, S., Boyden, J. E., & Webster, L. 2002, ApJS, 139, 259
Wang, Y.-M., Hawley, S. H., & Sheeley, N. R., Jr. 1996, Science, 271, 464
Wang, Y.-M., & Sheeley, N. R., Jr. 1990a, ApJ, 355, 726
———. 1990b, ApJ, 365, 372
———. 1992, ApJ, 392, 310
———. 1995, ApJ, 447, L143
Wang, Y.-M., & Sheeley, N. R., Jr. 2002, ApJ, 575, 542
———. 2003, ApJ, 599, 1404
———. 2004, ApJ, 612, 1196
Wang, Y.-M., Sheeley, N. R., Jr., & Lean, J. 2000, Geophys. Res. Lett., 27, 621
Wang, Y.-M., et al. 1998, ApJ, 508, 899
Zwickl, R. D., Roelof, E. C., Gold, R. E., Krimigis, S. M., & Armstrong, T. P. 1978, ApJ, 225, 281